Journal of Materials Chemistry C

ROYAL SOCIETY OF CHEMISTRY

COMMUNICATION

View Article Online
View Journal | View Issue

Cite this: J. Mater. Chem. C, 2021, 9, 6151

Received 5th March 2021,
Accepted 9th April 2021

DOI: 10.1039/d1tc01037a

rsc.li/materials-c

Stable down-conversion white light-emitting devices based on highly luminescent copper halides synthesized at room temperature†

Lin-Tao Wang, Zhuang-Zhuang Ma, Fei Zhang, Meng Wang, Xu Chen,* Di Wu, Yong-Tao Tian, Xin-Jian Li and Zhi-Feng Shi *

In recent years, the metal-halide perovskites have attracted intensive attention in the field of white light-emitting devices (WLEDs). However, their further commercial applications are severely hampered by the poor stability and lead toxicity of such materials. In this work, we demonstrate two types of lead-free ternary copper halides (blue-emissive $Cs_3Cu_2I_5$ and yellow-emissive $CsCu_2I_3$), which were synthesized by a convenient supersaturated recrystallization method at room temperature. Both materials have particularly good crystallinity and excellent stability against ultraviolet light, heat, and air oxygen/moisture. Temperature-dependent photoluminescence (PL) and time-resolved PL decay measurements confirm that the highly luminescent and largely Stokes-shifted broadband emission of both materials derived from the self-trapped exciton-related recombination. By using a mixture of $Cs_3Cu_2I_5$ and $CsCu_2I_3$ as the down-conversion phosphors, a high-performance WLED is demonstrated with the color coordinates of (0.324, 0.330), a correlated color temperature of 5877 K, and a color rendering index of 88.4. Also, a high luminous efficiency of 54.6 lm W^{-1} is realized, which is the highest value among the lead-free perovskite-based WLEDs. More importantly, the studied WLED demonstrates excellent operation stability, and almost no emission degradation occurs after continuously working for 100 h in air ambient. The results suggest that such ternary copper halides may be potentially attractive candidates for the fabrication of efficient, stable, and environmentally friendly WLEDs.

Introduction

In the era of increasing energy shortage, lighting accounts for almost 20% of global electricity consumption, so it is very necessary to develop efficient lighting methods.[1] Solid-state lighting in the form of white light-emitting devices (WLEDs) has higher power efficiency than traditional incandescent and fluorescent lamps, so it is the first choice for next-generation lighting equipment.[2–5] Currently, the commercial approach for WLED production is to combine blue LEDs with $Y_3Al_{15}O_{12}:Ge^{3+}$ yellow phosphors, because it has the advantages of low cost, simple structure, and high luminous efficiency (LE). However, the intense blue component in the white emission spectrum can damage the retina of humans, which limits the widespread applications of this technique.[6–9] Besides, this route is not sufficient to produce a high color rendering index (CRI) because the commonly used phosphors have a narrow excitation band and lack the red and green components in the spectrum. Therefore, a more friendly strategy for WLEDs is to use ultraviolet (UV) LED chips to stimulate a suitable broadband emission phosphor combination, which helps to improve the CRI and reduce the damage to the eyes caused by the undesired blue component.

Recently, metal-halide perovskites have rapidly advanced in down-conversion WLED applications, which benefits from their remarkable optical properties including high color purity, tunable fluorescence emission, high photoluminescence quantum yield (PLQY), and low-cost processing technique.[10–21] Since the first report by Snaith *et al.* in 2016, this field has made great progress.[22] However, there is still a lack of major breakthroughs in the process of commercializing WLEDs based on perovskites although numerous efforts have been made. The possible reasons can be summarized as follows.[23–27] Firstly, in light of the well-known hypersensitivity of lead-halide perovskites in the air with moisture, oxygen, heat, and UV light, they are easily decomposed and the luminescence will be severely attenuated. Secondly, the large-scale applications of WLEDs based on halide perovskites were limited by the undesirable lead toxicity. Thirdly, for the conventional two-component or multi-component strategy for device preparation, there are still some limitations and disadvantages that need to be taken seriously. For example, due to the self-absorption of photons

Key Laboratory of Materials Physics of Ministry of Education, School of Physics and Microelectronics, Zhengzhou University, Daxue Road 75, Zhengzhou 450052, China. E-mail: shizf@zzu.edu.cn, xchen@zzu.edu.cn; Fax: +86-371-67766629; Tel: +86-150-9333-9165

† Electronic supplementary information (ESI) available. See DOI: 10.1039/d1tc01037a

and the different degradation rates of phosphors, efficiency loss and color rendering changes will be caused after a long-term operation. Therefore, it is extensively urgent to explore non-toxic and highly stable alternatives as phosphors to solve the above issues.

It was firstly proposed to use Sn^{2+} or Ge^{2+} with similar diameter and electronic structure to Pb^{2+} as an on-site replacement in halide perovskites. Unfortunately, the perovskites based on Sn^{2+} or Ge^{2+} would be easily oxidized into their tetravalent state (Sn^{4+}, Ge^{4+}) in air.[28–32] Similar electronic properties can be obtained by using elements (Bi^{3+} and Sb^{3+}) adjacent to lead in the periodic table. Unfortunately, the experimental results have confirmed that the obtained PLQY of bismuth/antimony-based perovskites is still not satisfactory.[33–41] Compared with the above metal substitutions, copper has attracted the attention of researchers due to its non-toxicity, low cost, and abundant reserves. In our recent studies, blue-emissive $Cs_3Cu_2I_5$ and yellow-emissive $CsCu_2I_3$ were synthesized by solution methods and their applications in electrically driven LEDs were also demonstrated.[43] Both copper halides have high emission efficiency and are very stable in air ambient. Moreover, they are all characterized by broadband emission features and large Stokes shift, which brings us hope for fabricating a highly stable WLED because the color instability and photon self-absorption facing current multi-component WLED challenges can be avoided.

In this work, brightly luminescent and stable $Cs_3Cu_2I_5$ and $CsCu_2I_3$ were synthesized by the supersaturated recrystallization method at room temperature (RT). The entire visible light area can be covered because of their broadband emission characteristics. By using a mixture of $Cs_3Cu_2I_5$ and $CsCu_2I_3$ as the down-conversion phosphors, a high-performance WLED was fabricated with a CRI of 88.4 and a LE of 54.6 lm W^{-1}, which is currently the highest value among lead-free perovskite-based WLEDs. More importantly, the unencapsulated WLED in continuous current mode can efficiently sustain for 100 h without any emission decay, demonstrating remarkable operation stability. This research will provide new insights into the design of new white phosphors and diodes for next-generation lighting technologies.

Experimental section

Materials used in this experiment include cesium iodide (CsI, Xi'an Polymer Light Technology Corp., 99.9%), copper (I) iodide (CuI, SIGMA, 99.999%), dimethylformamide (DMF, $\geq$99.5%), dimethylsulfoxide (DMSO, $\geq$99.5%), isopropanol and chloroform. Each precursor and solvent was used without further purification.

Synthesis of $Cs_3Cu_2I_5$ microscale crystals

0.6 mmol CsI and 0.4 mmol CuI were dissolved in 2 mL of DMF and DMSO (1 : 1) mixed solution. For the synthesis of $Cs_3Cu_2I_5$ microscale crystals, 0.5 mL of the precursor solution was quickly dropped into chloroform (4 mL) under vigorous stirring. After a few-second reaction, a white precipitate was formed. Then, the solution was centrifuged at 10 000 rpm for 10 min to discard the supernatant. Finally, the $Cs_3Cu_2I_5$ powder was obtained for characterization.

Synthesis of $CsCu_2I_3$ microscale crystals

0.2 mmol CsI and 0.4 mmol CuI were dissolved in 2 mL of DMF and DMSO (1 : 1) mixed solution. For the synthesis of $CsCu_2I_3$ microscale crystals, 0.5 mL of the precursor solution was quickly dropped into isopropanol (4 mL) under vigorous stirring. After a few-second reaction, a yellow precipitate was formed. Then, the solution was centrifuged at 10 000 rpm for 10 min to discard the supernatant. Finally, the $CsCu_2I_3$ powder was obtained for characterization.

Fabrication of WLEDs

The as-prepared blue-emissive $Cs_3Cu_2I_5$ microscale crystals, yellow-emissive $CsCu_2I_3$ microscale crystals and silica gel were mixed in a 20 mL beaker to obtain a homogeneous latex. The WLEDs were fabricated by combining the latex with UV LED chips (310 nm). Then the device was solidified in a vacuum oven at 40 °C for 60 min, and at 110 °C for 1 h sequentially.

Characterizations

The microstructures of the as-synthesized products were characterized using a high-resolution transmission electron microscope (TEM, JEM-3010). The crystallinity characterizations of $Cs_3Cu_2I_5$ and $CsCu_2I_3$ microscale crystals were analyzed by X-ray diffraction (XRD, Panalytical X' Pert Pro). The morphologies and chemical compositions of the products were analyzed by scanning electron microscope (SEM, JSM-7500F) and energy dispersive X-ray spectroscopy (EDS). The optical properties of the products were measured by using a Shimadzu UV-3150 spectrophotometer and steady-state PL spectra (Horiba; Fluorolog-3) with an excitation line of 290 nm. A closed-cycle helium cryostat (Jannis; CCS-100) was used to carry out the PL measurement at different temperatures. The absolute PLQY of the $Cs_3Cu_2I_5$ and $CsCu_2I_3$ powder were measured by using a fluorescence spectrometer (Horiba; FluoroMax-4) with an integrated sphere (Horiba; Quanta-ϕ) with the excitation wavelength of 290 nm. For high-temperature PL measurement, the perovskite films were placed on a copper heat sink, the temperature of which can be controlled by a heating pane with a heating area of 40 mm $\times$ 40 mm. Absorption/PL of $Cs_3Cu_2I_5$ and $CsCu_2I_3$ was conducted with the films by spin-coating microscale crystals on quartz substrates. Excitation power and temperature-dependent PL were conducted with the thin film form by spin-coating the $Cs_3Cu_2I_5$ and $CsCu_2I_3$ microscale crystals on the SiO_2/Si substrates.

Results and discussion

In this experiment, a simple RT supersaturated recrystallization approach was employed to synthesize the $Cs_3Cu_2I_5$ and $CsCu_2I_3$ microscale crystals, and the corresponding processing procedures

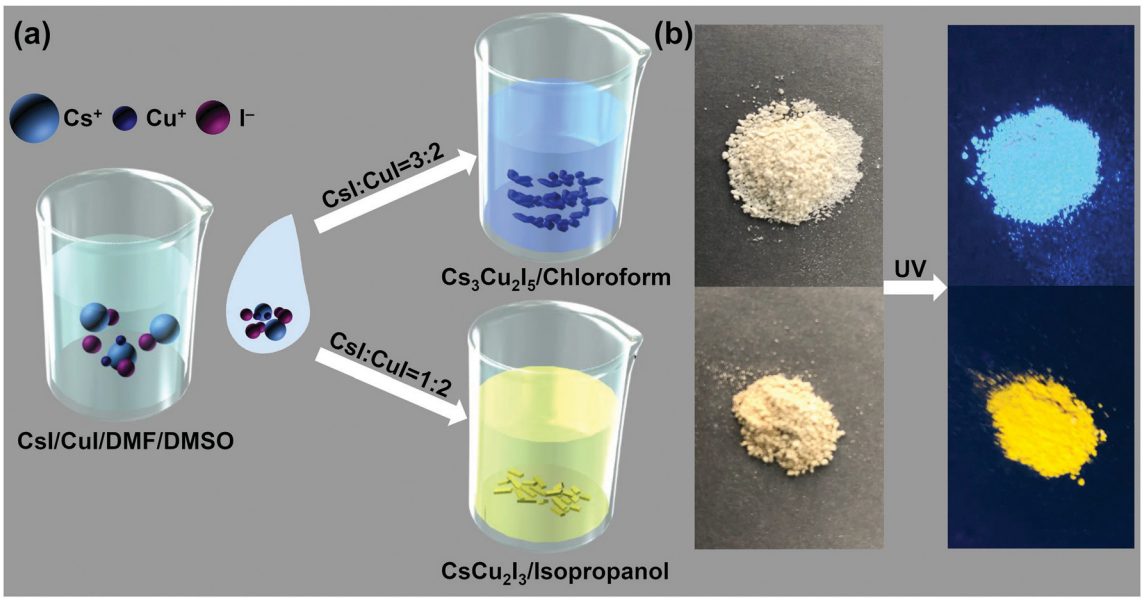

Fig. 1 (a) Schematic illustration of the reaction system for the supersaturated recrystallization technique at RT. (b) Photographs of synthesized $Cs_3Cu_2I_5$ and $CsCu_2I_3$ powders under sunlight (left) and 254 nm UV light irradiation (right).

are illustrated in Fig. 1a. First, for the $Cs_3Cu_2I_5$ microscale crystals, a mixture of CsI and CuI in a molar ratio of 3 : 2 was dissolved in DMF and DMSO "good" solvent to form a clear precursor solution. Then, the precursor solution was quickly dropped into the chloroform solution, which was the "poor" solvent for these precursor ions. Under vigorous stirring, a highly supersaturated state is immediately triggered and a rapid recrystallization reaction occurs. Finally, the solid powders of $Cs_3Cu_2I_5$ microscale crystals were purified and obtained by a centrifugation process. It is worth noting that the whole synthesis process is completed at RT under ambient conditions without the requirements of high temperature and inert gas protection, which greatly reduces the preparation cost and complexity. The preparation procedures of the $CsCu_2I_3$ microscale crystals are similar to the above processes, except that the molar ratio of CsI and CuI is 1 : 2 and the "poor" solvent is isopropanol. The right panes of Fig. 1b display the typical optical images of the as-synthesized $Cs_3Cu_2I_5$ and $CsCu_2I_3$ powders under ambient conditions and UV lamp (254 nm) irradiation, respectively. The observed strong and uniform blue and yellow light suggest that the $Cs_3Cu_2I_5$ and $CsCu_2I_3$ powders have excellent luminescence properties, implying their potential as down-conversion phosphors for the construction of optically excited LEDs.

The morphology properties of $Cs_3Cu_2I_5$ and $CsCu_2I_3$ products were characterized by the SEM and TEM measurements. As shown in Fig. 2a and d, the typical $Cs_3Cu_2I_5$ products exhibit an elongated rod-shaped morphology with a length of ~7 μm and a width of ~1 μm, while the $CsCu_2I_3$ products show a flat column-shaped morphology with a length of ~15 μm and a width of ~2 μm. Fig. 2b and e show their chemical element mapping results measured by EDS, in which the Cs, Cu and I elements are homogeneously distributed for both materials. Fig. S1 and S2 (ESI†) show the corresponding EDS spectra, which yield the Cs : Cu : I atomic ratios of 3.00 : 2.05 : 5.05 in $Cs_3Cu_2I_5$ and 1.00 : 2.03 : 3.05 in $CsCu_2I_3$, close to the stoichiometry of the anticipated composition. Fig. 2d and f present the TEM images of the $Cs_3Cu_2I_5$ and $CsCu_2I_3$ microscale crystals, which all have quite smooth surfaces with uniform diameter along the growth direction. The in-plane structural information of them was revealed by the selected-area electron diffractions (SAED). As depicted in the insets of Fig. 2c and f, the diffraction spots could be assigned to the (130) and (340) crystal planes projecting along the [005] orientation of $Cs_3Cu_2I_5$ microscale crystals; for the $CsCu_2I_3$ microscale crystals, the spots can be indexed to the (020) and (002) crystal planes projecting along the [400] orientation. Note that the high-quality SAED patterns for $Cs_3Cu_2I_5$ and $CsCu_2I_3$ verify their single-crystalline features. XRD measurements were further performed to investigate the structural characteristics of $CsCu_2I_3$ and $Cs_3Cu_2I_5$ microscale crystals. As shown in Fig. 2g and h, the diffraction peaks of the two samples correspond well to the standard diffractions, in which the dominant diffraction peaks at 24.02°, 25.57°, 26.34°, and 30.60° can be assigned to the (122), (320), (222), and (004) planes of orthorhombic $Cs_3Cu_2I_5$, and the peaks at 10.77°, 13.45°, 21.96°, 26.19°, and 29.39° can be ascribed to the (110), (020), (130), (221), and (002) planes of orthorhombic $CsCu_2I_3$. It should be mentioned that no other peaks (*e.g.*, CsI, CuI) were detected above the detection limit, suggesting a high phase purity of two samples. To analyze the optical properties of two samples, UV-visible absorption and steady-state PL spectra were measured. As shown in Fig. 2i, the absorption edge of $CsCu_2I_3$ is around 330 nm, whereas that for $Cs_3Cu_2I_5$ is blue-shifted to approximately 305 nm. In addition, both $Cs_3Cu_2I_5$ and $CsCu_2I_3$ are characterized by large Stokes shifts ($CsCu_2I_3$, 228 nm; $Cs_3Cu_2I_5$, 139 nm) and large linewidths ($CsCu_2I_3$, 115 nm; $Cs_3Cu_2I_5$, 85 nm), which is typical in the case

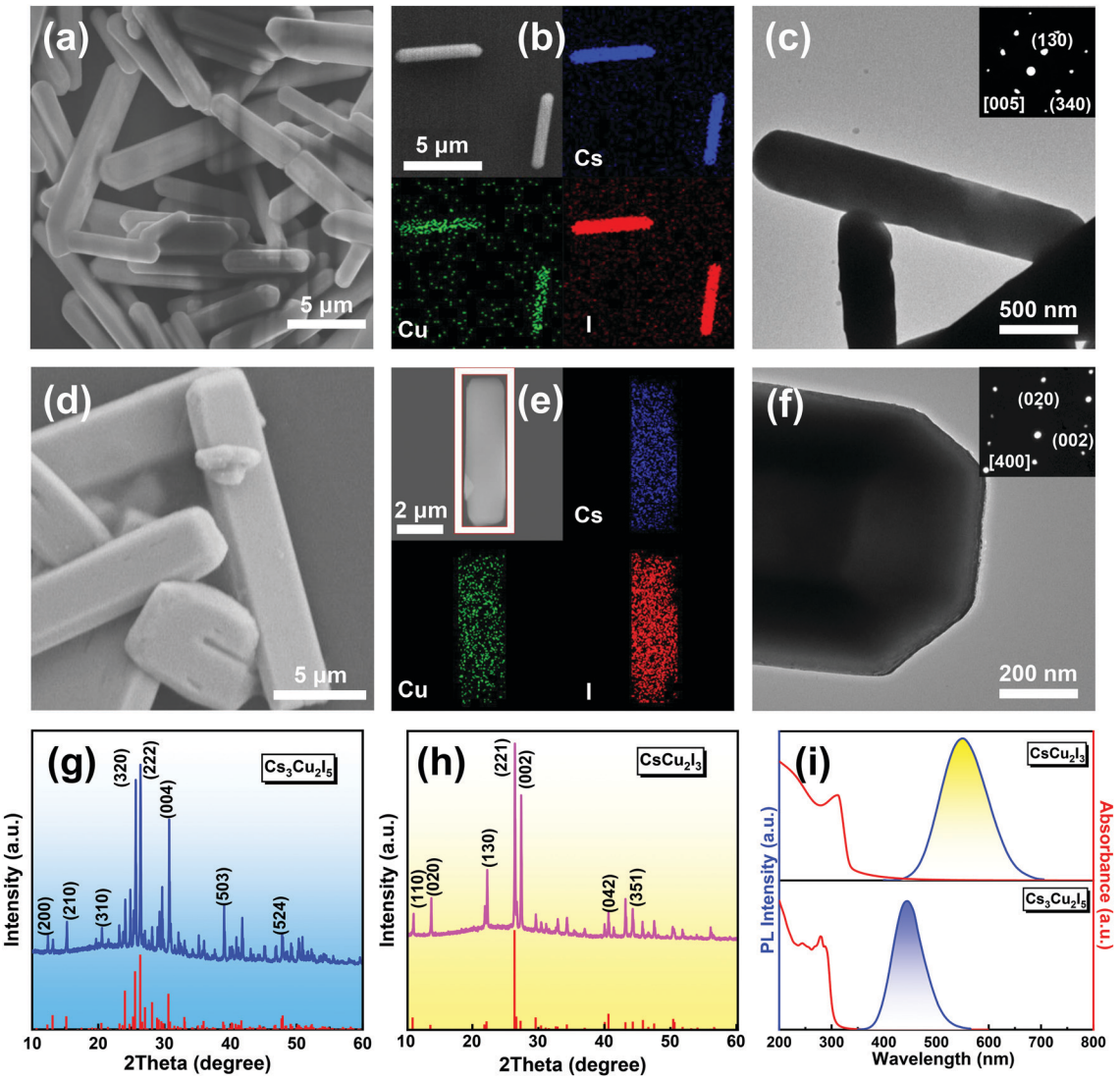

Fig. 2 SEM images of (a) $Cs_3Cu_2I_5$ and (d) $CsCu_2I_3$ microscale crystals, and the corresponding EDS elemental mapping of (b) $Cs_3Cu_2I_5$ and (e) $CsCu_2I_3$. TEM images of (c) $Cs_3Cu_2I_5$ and (f) $CsCu_2I_3$ microscale crystals. The insets show the SAED patterns. Experimental XRD patterns of (g) $Cs_3Cu_2I_5$ and (h) $CsCu_2I_3$ microscale crystals. (i) Absorption and PL spectra of the as-prepared $CsCu_2I_3$ and $Cs_3Cu_2I_5$ microscale crystals.

of self-trapped exciton (STE)-related transition,[44–48] which will be discussed later. The broadband emission and large Stokes shifts for two copper halides imply that the efficiency losses and color instability issues of WLEDs induced by the photon self-absorption can be effectively suppressed. We then measured the absolute PLQY of the obtained two samples, and the values of 89% for $Cs_3Cu_2I_5$ and 15% for $CsCu_2I_3$ were obtained.

In order to better understand the optical recombination mechanism of the two samples, temperature-dependent PL measurements were carried out with the temperature ranging from 10 to 300 K. It can be observed that the relative PL intensity of both samples exhibits a significant temperature quenching behavior with the increase of temperature, as shown in Fig. 3a and d, which can be assigned to the thermally activated nonradiative recombination process. Then the exciton binding energy (E_b) of $Cs_3Cu_2I_5$ and $CsCu_2I_3$ microscale crystals can be obtained by the following equation:

$$I(T) = \frac{I_0}{1 + A\exp\left(-\frac{E_b}{k_B T}\right)} \quad (1)$$

where $I(T)$ and I_0 are the integrated PL intensities at temperature T and 0 K, respectively. E_b is the exciton binding energy, and k_B is the Boltzmann constant. For $Cs_3Cu_2I_5$ and $CsCu_2I_3$ microscale crystals, the E_b were calculated to be 139.3 and 234.4 meV (Fig. 3b and e), respectively, which were much larger than that of traditional perovskite materials.[43,49] Such a large E_b can ensure the generation of excitons at RT and promote their efficient radiative recombination, and hence the samples are prone to exhibit strong PL intensity. Moreover, their Huang–Rhys factor (S) and the optical phonon frequency ($\hbar\omega_{phonon}$) were calculated to reveal the exciton–phonon

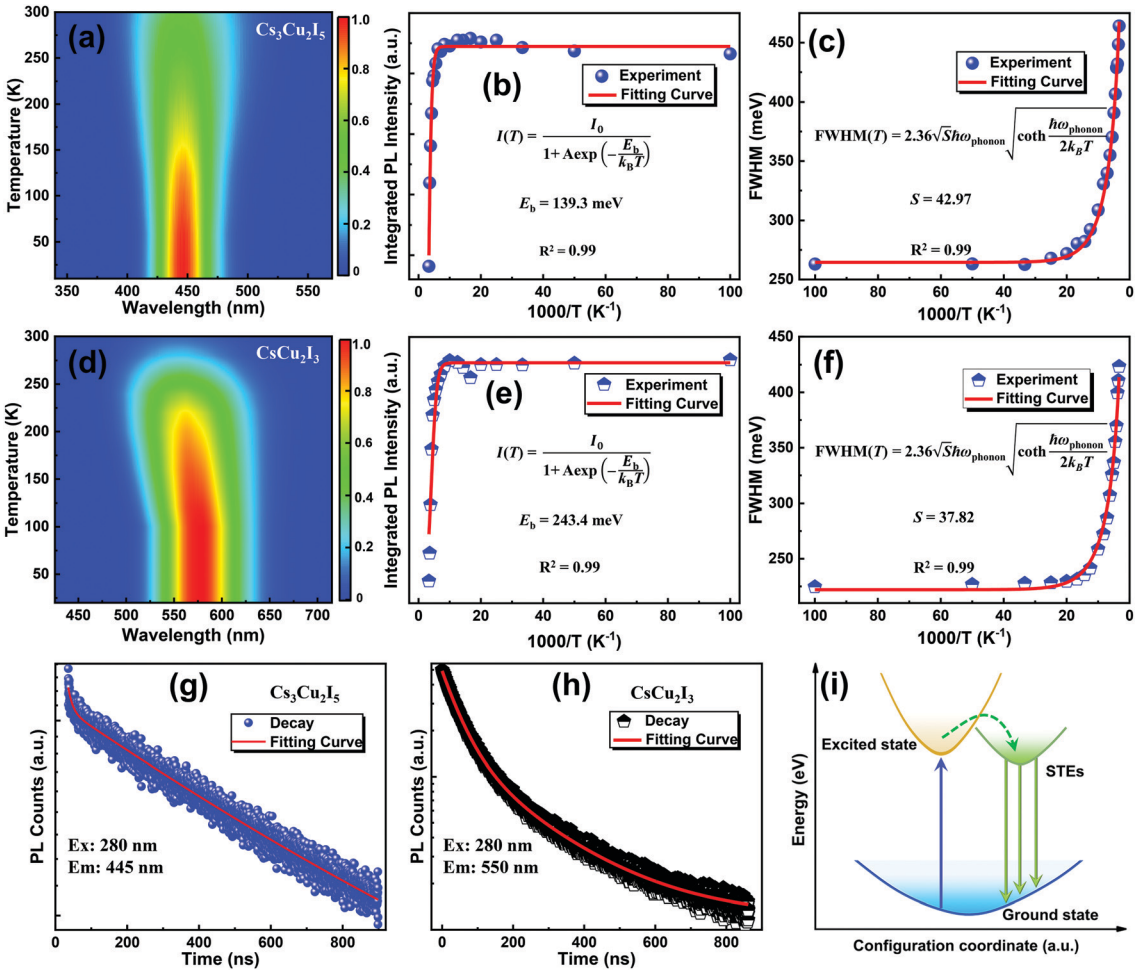

Fig. 3 Pseudocolor maps of temperature-dependent PL spectra of (a) $Cs_3Cu_2I_5$ and (d) $CsCu_2I_3$ microscale crystals ranging from 10 to 300 K. Integrated PL intensity of (b) $Cs_3Cu_2I_5$ and (e) $CsCu_2I_3$ microscale crystals as a function of reciprocal temperature. FWHM of (c) $Cs_3Cu_2I_5$ and (f) $CsCu_2I_3$ microscale crystals as a function of reciprocal temperature. Time-resolved PL decay and fitting curves of (g) $Cs_3Cu_2I_5$ and (h) $CsCu_2I_3$ microscale crystals. (i) Configuration coordinate diagram for the STEs' dynamic mechanism of the $Cs_3Cu_2I_5$ and $CsCu_2I_3$.

coupling of two materials by the following equation:

$$\mathrm{FWHM}(T) = 2.36\sqrt{S}\hbar\omega_{\mathrm{phonon}}\sqrt{\coth\frac{\hbar\omega_{\mathrm{phonon}}}{2k_{\mathrm{B}}T}} \qquad (2)$$

Through fitting the temperature-dependent full-width at high-maximum (FWHM) curve, the S factors of $Cs_3Cu_2I_5$ and $CsCu_2I_3$ were extracted as 42.92 and 37.82, and the $\hbar\omega_{\mathrm{phonon}}$ were 17.54 and 15.29 meV, respectively, as shown in Fig. 3c and f. Note that the obtained S factor is much higher than that of many traditional materials with free exciton recombination features, which indicates the presence of strong electron–phonon coupling in both samples, and facilitates the formation of STEs.[50,51] As shown in Fig. S3a and b (ESI†), the PL excitation spectra of $Cs_3Cu_2I_5$ and $CsCu_2I_3$ exhibit identical shape and peak position, which suggests that their broadband emission originates from the relaxation of the same excited state.[2,50,52] Besides, time-resolved PL measurements of $Cs_3Cu_2I_5$ and $CsCu_2I_3$ were performed, and the obtained results and fitting curves are plotted in Fig. 3g and h. It can be seen that the average lifetimes of $Cs_3Cu_2I_5$ and $CsCu_2I_3$ are 638 ns and 102 ns. These results are similar to other studies on copper-based halides with STE emission features.[48–52] In view of the above discussions, the excitation and recombination processes of both samples can be illustrated in the coordinate diagram. As shown in Fig. 3i, upon photoexcitation, electrons are excited from the ground state to the high-energy excitation state, and then are trapped into the intrinsic lower-energy self-trapped states due to the strong electron–phonon coupling effect in $Cs_3Cu_2I_5$ and $CsCu_2I_3$. Consequently, the radiative recombination from self-trapped states generates a highly bright broadband emission with large Stokes shifts and long lifetimes.

It is well known that the stability of lead-halide perovskites has always been a challenge, which is the main obstacle hindering their potential applications significantly. In this study, a comprehensive stability investigation was conducted on two materials by evaluating the influences of heat, UV light irradiation, and long-term storage on their optical and structural characteristics. Firstly, we conducted the thermal cycling PL tests

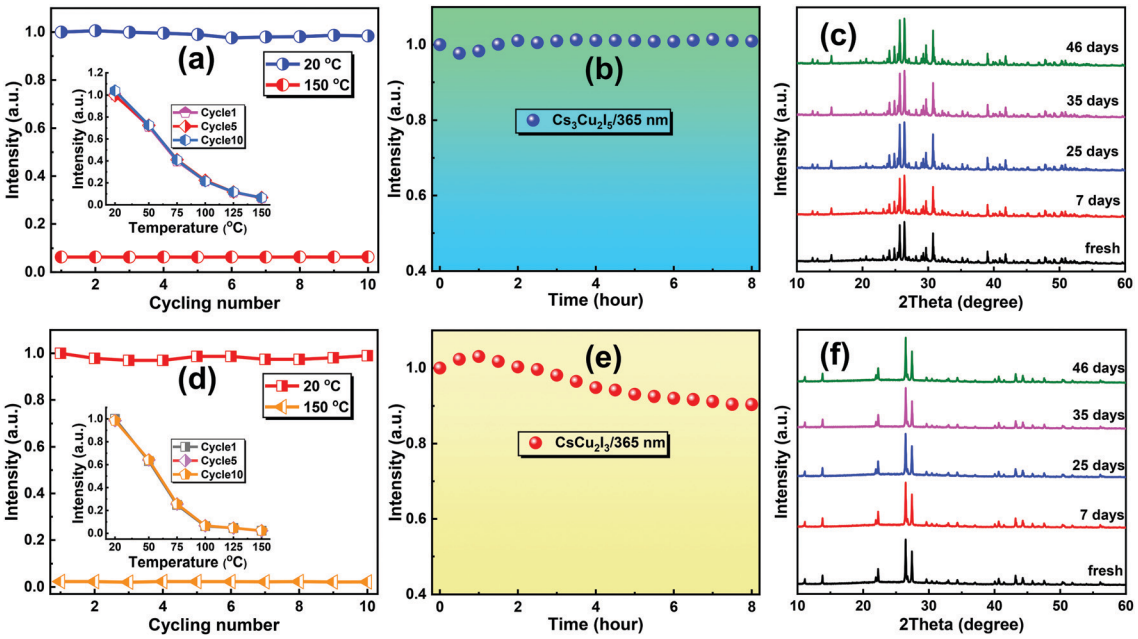

Fig. 4 Relative emission intensity of (a) $Cs_3Cu_2I_5$ and (d) $CsCu_2I_3$ microscale crystals at two representative temperature points (20 °C and 150 °C) over ten thermal cycling measurements. The insets show the emission intensity change of different cycles. Photostability test of the (b) $Cs_3Cu_2I_5$ and (e) $CsCu_2I_3$ microscale crystals under UV light irradiation (365 nm, 8 W). XRD patterns of (c) $Cs_3Cu_2I_5$ and (f) $CsCu_2I_3$ microscale crystals after different storage periods in air ambient (25 °C, 55% humidity).

in the temperature range of 20–150 °C, and the relative PL intensities at two representative temperature points (20 °C and 150 °C) are summarized in Fig. 4a and d. One can see that the relative PL intensity of both materials exhibits almost no obvious decay over ten heating/cooling cycles, with the peak intensity, spectral shape and peak position unchanged (Fig. S4, ESI†), greatly superior to the previous studies on conventional lead-based halides.[10–12] This recoverable emission behavior of $Cs_3Cu_2I_5$ and $CsCu_2I_3$ after high temperature aging is a sign of their good thermal stability. Secondly, the photostability test of two materials was further conducted by continuously illuminating them with a portable UV lamp at a 10 cm distance, and the emission performance was quantitatively studied by monitoring the evolution of PL with time. As shown in Fig. 4b and e, the emission intensity of $Cs_3Cu_2I_5$ can be almost maintained under continuous UV light irradiation for 8 h. Under the same conditions, a slight emission decay of about 10% occurs for $CsCu_2I_3$, which may be caused by the undesired photo-oxidation effect, as observed in conventional lead-based perovskites.[12] Fig. S5a and b (ESI†) show the corresponding PL spectra of $Cs_3Cu_2I_5$ and $CsCu_2I_3$ recorded at different illumination time intervals. Except for the slight change in peak intensity (only for $CsCu_2I_3$), the FWHM and shape of the PL spectra are almost unchanged. Besides, the long-term storage stability of $Cs_3Cu_2I_5$ and $CsCu_2I_3$ microscale crystals, without any protection and encapsulation, was studied by intermittently recording their XRD patterns after different storage periods in air ambient (25 °C, 50–60% humidity). As shown in Fig. 4c and f, both samples show good structural stability, which preserves their structural integrity after 46 day storage without the appearance of additional impurity diffraction peaks. The above results indicate remarkable stability of both $Cs_3Cu_2I_5$ and $CsCu_2I_3$ microscale crystals against heat, UV light, and environment oxygen/moisture, and are also evidence of the reliable copper halides as down-conversion phosphors compatible for WLED applications under harsh conditions.

The combination of low toxicity, high emission efficiency, and excellent stability of two copper halides suggests their promising potential applications in lighting fields. Moreover, the blue-emissive $Cs_3Cu_2I_5$ and yellow-emissive $CsCu_2I_3$ with large Stoke shifts and broadband emission can avoid the photon self-absorption phenomenon of the device to the greatest extent, and thus good color rendering and reliable operation stability can be expected. In the present case, single-color LEDs and WLEDs were constructed by encapsulating $Cs_3Cu_2I_5$ and $CsCu_2I_3$ powders and their mixtures as the down-conversion phosphors on a commercial UV LED chip (310 nm) for blue LED, yellow LED, and WLED fabrication, respectively. Fig. S6 (ESI†) shows the schematic structure of the proposed devices, in which the upper phosphor layer is separated from the bottom excitation UV LED. Due to the appreciable distance between the phosphors and LED chip, the heat released from the bottom LED chip is rarely applied to the upper phosphors, so that the efficient light emission can be maintained for a long time. Fig. 5a–c show the typical photographs of three working devices under the same driving current of 5 mA, and strong blue, yellow, and white light can be observed. Fig. 5d–f display the emission spectra of the blue LED, yellow LED, and WLED operated at different currents, and their emission characteristics are well-matched with the PL spectra of $Cs_3Cu_2I_5$ and $CsCu_2I_3$, respectively.

Another observed phenomenon is that the emission intensity of three devices exhibits a monotonic increase, without premature saturation toward UV light excitation, which also indicates the

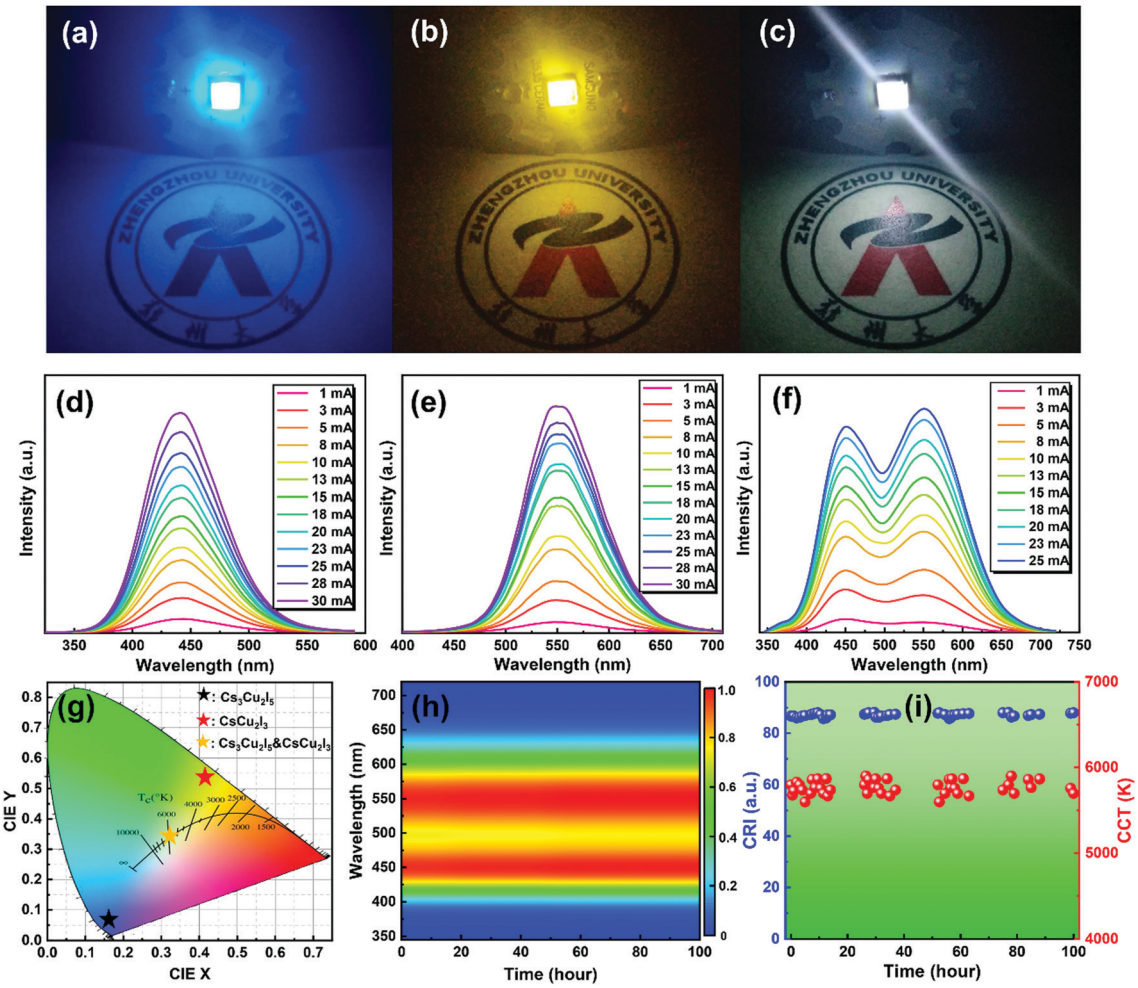

Fig. 5 Photographs of UV-pumped (a) blue LED and yellow LED based on $Cs_3Cu_2I_5$ and $CsCu_2I_3$ phosphors, respectively. (c) Photograph of a working WLED by using mixtures of $Cs_3Cu_2I_5$ and $CsCu_2I_3$ as the phosphors. Emission spectra of (d) blue LED, (e) yellow LED, and (f) WLED at different driving currents. (g) CIE color coordinates of the blue LED, yellow LED, and WLED. (h) PL spectra, (i) CRI and CCT of the WLED after different running periods under the driving current of 5 mA, showing its good operation stability.

good color chromatics stability of three devices and the photostability of both phosphors. Fig. 5g plots the Commission International de l'Eclairage (CIE) color coordinates of three devices, in which the blue LED, yellow LED, and WLED are located at (0.161, 0.072), (0.423, 0.533), and (0.324, 0.330), respectively. Besides, other key device parameters for the WLED including the correlated color temperature (CCT), CRI, and LE were also measured to be 5877 K, 88.4, and 54.6 lm W^{-1}, respectively. Note that the high LE (54.6 lm W^{-1}) obtained is a new record for lead-free perovskite-based WLEDs. Table 1 summarizes the device performances of the studied WLEDs and other reported devices constructed by a single or multi-component strategy, and the value of luminous efficiency in our case is the highest among the lead-free perovskite-based WLEDs.

It is generally accepted that the long-term operation stability of perovskite-based optoelectronic devices has always been criticized. To assess the suitability of the studied WLED to practical applications, the preliminary stability study of the device was therefore conducted by tracking the evolution of the emission spectra with running time, in which a continuous current of 5 mA was fixed and the emission spectra were captured intermittently in air ambient (25 °C, 55% humidity).

Table 1 Summary of the device performances of the prepared WLEDs

Emitter	Lead-free (yes/no)	CRI	CCT (K)	LE (lm W^{-1})	Lifetime (h)	Ref.
$C_3N_2H_{12}PbBr_4$	No	82	4669	—	—	18
$(EDBE)PbBr_4$	No	—	6519	—	>7	19
α-$(DMEN)PbBr_4$	No	73	7863	—	—	20
$CsPbBr_3/CsPbBr_{1.2}I_{1.8}$	No	—	—	61.2	10	21
$(C_6H_5C_2H_4NH_3)_2PbCl_4$	No	84	4426	—	—	15
$CsPbBr_3/CsPbBr_{1.2}I_{1.8}$	No	82	5853	14.1	—	16
$[PbF][(CH_2)_4(CO_2)_2]_{0.5}$	No	78	5620	—	—	17
$Cs_3Bi_2Br_9$	Yes	—	—	—	—	33
$(OCTAm)_2SnBr_4$	Yes	89	6530	—	—	38
$(Cs_4N_2H_{14}Br)_4SnBrxI_{6-x}$	Yes	84	5632	32.2	>12	41
$(C_4N_2H_{14}Br)_4SnBr_6$	Yes	70	4946	—	>7	42
$Cs_3Cu_2I_5/CsCu_2I_3$	Yes	89.4	5877	54.6	>100	This work

As shown in Fig. 5h, after continuous running for 100 h, there is no change of the emission performance for the studied WLEDs, involving the spectral shape, peak position, and emission intensity, suggesting superior operation stability of the proposed WLED based on $Cs_3Cu_2I_5$ and $CsCu_2I_3$ mixtures. Moreover, the CCT and CRI of the WLEDs were also continuously collected, showing no obvious changes with the running time, as summarized in Fig. 5i. In addition, we found that the CIE of the WLED remained basically unchanged over a long working period, as seen in Fig. S7 (ESI†). Together with the environmentally friendly nature and facile processing method, the lead-free ternary copper halides can therefore be regarded as promising candidates as reliable down-conversion phosphors for high-performance WLED applications.

Conclusions

In conclusion, a stable and high-efficiency WLED by using blue-emissive $Cs_3Cu_2I_5$ and yellow-emissive $CsCu_2I_3$ as the down-conversion phosphors was successfully demonstrated, which were synthesized by a facile supersaturated recrystallization method at RT. The broadband emission feature of $Cs_3Cu_2I_5$ and $CsCu_2I_3$ allows their combined spectrum to cover the entire visible light region, and their large Stokes shift effectively avoids the undesired photon self-absorption and color instability issues benefited from the STE-related recombination mechanisms. The device performance of the studied WLED is remarkable in terms of a large CRI of 88.4 and a high LE of 54.6 lm W^{-1}, which is the highest value among the lead-free perovskite-based WLEDs as far as we know. More importantly, the unencapsulated WLED in continuous current mode can efficiently sustain for 100 h without any emission decay, demonstrating remarkable stability. The results obtained highlight the great potential of lead-free $Cs_3Cu_2I_5$ and $CsCu_2I_3$ as environmentally friendly and stable phosphors for high-performance WLEDs compatible with practical applications.

Author contributions

Z. S. and X. C. conceived the idea for detailed experiments. L. W., Z. M. and M. W. performed the material synthesis experiments. F. Z. and M. W. carried out the TEM, SEM, and XRD measurements. L. W. and M. W. performed the PL measurements. D. W., X. C., Y. T. and X. L. analyzed the data. The paper was written by L. W., and Z. S. guided the whole project.

Conflicts of interest

There are no conflicts to declare.

Acknowledgements

This work was supported by the National Natural Science Foundation of China (No. 11774318, 12074347, 12004346, and 61935009) and the Open Fund of the State Key Laboratory of Integrated Optoelectronics (IOSKL2020KF04).

Notes and references

1 Y. Sun, N. C. Giebink, H. Kanno, B. Ma, M. E. Thompson and S. R. Forrest, *Nature*, 2006, **440**, 908–912.
2 R. Lin, Q. Guo, Q. Zhu, Y. Zhu, W. Zheng and F. Huang, *Adv. Mater.*, 2019, **31**, 1905079.
3 M. K. Choi, J. Yang, K. Kang, D. Kim, C. Choi, C. Park, S. Kim, S. Chae, T. Kim, J. Kim, T. Hyeon and D. H. Kim, *Nat. Commun.*, 2015, **6**, 7149.
4 Z. Ma, Z. Shi, D. Yang, Y. Li, F. Zhang, L. Wang, X. Chen, D. Wu, Y. Tian, Y. Zhang, L. Zhang, X. Li and C. Shan, *Adv. Mater.*, 2021, **33**, 2001367.
5 Z. Wang, F. Yuan, X. Li, Y. Li, H. Zhong, L. Fan and S. Yang, *Adv. Mater.*, 2017, **29**, 1702910.
6 X. Zhuang, H. Zhang, K. Ye, Y. Liu and Y. Wang, *ACS Appl. Mater. Interfaces*, 2016, **8**, 11221–11225.
7 T. Lougheed, *Environ. Health Perspect.*, 2014, **122**, A81.
8 R. Albert and E. Joan, *Photobiology*, 2012, **88**, 1320–1345.
9 I. Jaadane, P. Boulenguez, S. Chahory, S. Carre, M. Savoldelli, L. Jonet, F. Behar-Cohen, C. Martinsons and A. Torriglia, *Free Radic. Biol. Med.*, 2015, **84**, 373–384.
10 L. Wang, Z. Shi, Z. Ma, D. Yang, F. Zhang, X. Ji, M. Wang, X. Chen, G. Na, S. Chen, D. Wu, Y. Zhang, X. Li, L. Zhang and C. Shan, *Nano Lett.*, 2020, **20**, 3568–3576.
11 L. Protesescu, S. Yakunin, M. I. Bodnarchuk, F. Krieg, R. Caputo, C. H. Hendon, R. X. Yang, A. Walsh and M. V. Kovalenko, *Nano Lett.*, 2015, **15**, 3692–3696.
12 X. Li, Y. Wu, S. Zhang, B. Cai, Y. Gu, J. Song and H. Zeng, *Adv. Funct. Mater.*, 2016, **26**, 2435–2445.
13 Q. A. Akkerman, V. D'Innocenzo, S. Accornero, A. Scarpellini, A. Petrozza, M. Prato and L. Manna, *J. Am. Chem. Soc.*, 2015, **137**, 10276–10281.
14 Z. Shi, Y. Li, Y. Zhang, Y. Chen, X. Li, D. Wu, T. Xu, C. Shan and G. Du, *Nano Lett.*, 2017, **17**, 313–321.
15 K. Thirumal, W. Chong, W. Xie, R. Ganguly, S. K. Muduli, M. Sherburne, M. Asta, S. Mhaisalkar, T. Sum, H. S. Soo and N. Mathews, *Chem. Mater.*, 2017, **29**, 3947–3953.
16 X. Di, J. Jiang, Z. Hu, L. Zhou, P. Li, S. Liu, W. Xiang and X. Liang, *Dyes Pigm.*, 2017, **146**, 361–367.
17 Z. Zhuang, C. Peng, G. Zhang, H. Yang, J. Yin and H. Fei, *Angew. Chem., Int. Ed.*, 2017, **56**, 14411–14416.
18 E. R. Dohner, E. T. Hoke and H. I. Karunadasa, *J. Am. Chem. Soc.*, 2014, **136**, 1718–1721.
19 Z. Yuan, C. Zhou, J. Messier, Y. Tian, Y. Shu, J. Wang, Y. Xin and B. Ma, *Adv. Opt. Mater.*, 2016, **4**, 2009–2015.
20 L. Mao, Y. Wu, C. C. Stoumpos, M. R. Wasielewski and M. G. Kanatzidis, *J. Am. Chem. Soc.*, 2017, **139**, 5210–5215.
21 C. Sun, Y. Zhang, C. Ruan, C. Yin, X. Wang, Y. Wang and W. W. Yu, *Adv. Mater.*, 2016, **28**, 10088–10094.
22 S. Pathak, N. Sakai, F. W. R. Rivarola, S. D. Stranks, J. Liu, G. Eperon, C. Ducati, K. Wojciechowski, J. T. Griffiths, A. A. Haghighirad, A. Pellaroque, H. Friend and H. J. Snaith, *Chem. Mater.*, 2015, **27**, 8066–8075.
23 X. G. Zhao, J. H. Yang, Y. Fu, D. Yang, Q. Xu, L. Yu, S. H. Wei and L. Zhang, *J. Am. Chem. Soc.*, 2017, **139**, 2630–2638.

24 F. Zhang, Z. F. Shi, Z. Z. Ma, Y. Li, S. Li, D. Wu, T. T. Xu, X. J. Li, C. X. Shan and G. T. Du, *Nanoscale*, 2018, **10**, 20131–20139.
25 M. Leng, Z. Chen, Y. Yang, Z. Li, K. Zeng, K. Li, G. Niu, Y. He, Q. Zhou and J. Tang, *Angew. Chem., Int. Ed.*, 2016, **55**, 15012–15016.
26 L. Lei, D. Chen, C. Li, F. Huang, J. Zhang and S. Xu, *J. Mater. Chem. C*, 2018, **6**, 5427–5433.
27 A. Loiudice, S. Saris, E. Oveisi, D. T. L. Alexander and R. Buonsanti, *Angew. Chem., Int. Ed.*, 2017, **56**, 10696–10701.
28 A. Babayigit, D. Thanh, A. Ethirajan, J. Manca, M. Muller, H. G. Boyen and B. Conings, *Sci. Rep.*, 2016, **6**, 18721.
29 S. Shao, J. Liu, G. Portale, H. H. Fang, G. R. Blake, G. H. Brink, L. J. A. Koster and M. A. Loi, *Adv. Energy Mater.*, 2018, **8**, 1702019.
30 Z. Ma, L. Wang, X. Ji, X. Chen and Z. Shi, *J. Phys. Chem. Lett.*, 2020, **11**, 5517–5530.
31 B. Saparov, J. P. Sun, W. Meng, Z. Xiao, H. S. Duan, O. Gunawan, D. Shin, I. G. Hill, Y. Yan and D. B. Mitzi, *Chem. Mater.*, 2016, **28**, 2315–2322.
32 A. Wang, Y. Guo, Z. Zhou, X. Niu, Y. Wang, F. Muhammad, H. Li, T. Zhang, J. Wang and Z. Deng, *Chem. Sci.*, 2019, **10**, 4573–4579.
33 M. Leng, Y. Yang, K. Zeng, Z. Chen, Z. Tan, S. Li, J. Li, B. Xu, D. Li, M. P. Hautzinger, Y. Fu, T. Zhai, L. Xu, G. Niu, S. Jin and J. Tang, *Adv. Funct. Mater.*, 2018, **28**, 1704446.
34 H. Shao, X. Bai, H. Cui, G. Pan, P. Jing, S. Qu, J. Zhu, Y. Zhai, B. Dong and H. Song, *Nanoscale*, 2018, **10**, 1023–1029.
35 Z. Ma, Z. Shi, L. Wang, F. Zhang, D. Wu, D. Yang, X. Chen, Y. Zhang, C. Shan and X. Li, *Nanoscale*, 2020, **12**, 3637–3645.
36 J. Zhang, Y. Yang, H. Deng, U. Farooq, X. Yang, J. Khan, J. Tang and H. Song, *ACS Nano*, 2017, **11**, 9294–9302.
37 K. M. McCall, C. C. Stoumpos, S. S. Kostina, M. G. Kanatzidis and B. W. Wessels, *Chem. Mater.*, 2017, **29**, 4129–4145.
38 J. Sun, J. Yang, J. I. Lee, J. H. Cho and M. S. Kang, *J. Phys. Chem. Lett.*, 2018, **9**, 1573–1583.
39 C. Zuo and L. Ding, *Angew. Chem., Int. Ed.*, 2017, **129**, 6628–6632.
40 Z. Z. Ma, Z. F. Shi, D. Yang, F. Zhang, S. Li, L. Wang, D. Wu, Y. Zhang, G. Na, L. Zhang, X. Li, Y. Zhang and C. X. Shan, *ACS Energy Lett.*, 2020, **5**, 385–394.
41 C. K. Zhou, Y. Tian, Z. Yuan, H. R. Lin, B. H. Chen, R. Clark, T. Dilbeck, Y. Zhou, J. Hurley, J. Neu, T. Besara, T. Siegrist, P. Djurovich and B. W. Ma, *ACS Appl. Mater. Interfaces*, 2017, **9**, 44579–44583.
42 C. Zhou, H. Lin, Y. Tian, Z. Yuan, R. Clark, B. Chen, L. J. van de Burgt, J. C. Wang, Y. Zhou, K. Hanson, Q. J. Meisner, J. Neu, T. Besara, T. Siegrist, E. Lambers, P. Djurovich and B. Ma, *Chem. Sci.*, 2018, **9**, 586–593.
43 Z. Ma, Z. Shi, C. Qin, M. Cui, D. Yang, X. Wang, L. Wang, X. Ji, X. Chen, J. Sun, D. Wu, Y. Zhang, X. Li, L. Zhang and C. Shan, *ACS Nano*, 2020, **14**, 4475–4486.
44 Z. Shi, S. Li, Y. Li, H. Ji, X. Li, D. Wu, T. Xu, Y. Chen, Y. Tian, Y. Zhang, C. Shan and G. Du, *ACS Nano*, 2018, **12**, 1462–1472.
45 M. A. Halcrow, *Chem. Soc. Rev.*, 2013, **42**, 1784–1795.
46 B. Murali, S. Dey, A. L. Abdelhady, W. Peng, E. Alarousu, A. R. Kirmani, N. Cho, S. P. Sarmah, M. R. Parida, M. I. Saidaminov, A. A. Zhumekenov, J. Sun, M. S. Alias, E. Yengel, B. S. Ooi, A. Amassian and O. M. Bakr, and O. F. Mohammed, *ACS Energy Lett.*, 2016, **1**, 1119–1126.
47 V. K. Ravi, G. B. Markad and A. Nag, *ACS Energy Lett.*, 2016, **1**, 665–671.
48 Z. Xiao, K. Z. Du, W. Meng, D. B. Mitzi and Y. Yan, *Angew. Chem., Int. Ed.*, 2017, **129**, 12275–12279.
49 J. Luo, X. Wang, S. Li, J. Liu, Y. Guo, G. Niu, L. Yao, Y. Fu, L. Gao, Q. Dong, C. Zhao, M. Leng, F. Ma, W. Liang, L. Wang, S. Jin, J. Han, L. Zhang, J. Etheridge, J. Wang, Y. Yan, E. H. Sargent and J. Tang, *Nature*, 2018, **563**, 541–545.
50 Y. E. Kim, J. Kim, J. W. Park, K. Park and Y. Lee, *Chem. Commun.*, 2017, **53**, 2858–2861.
51 Y. Li, Z. Shi, W. Liang, L. Wang, S. Li, F. Zhang, Z. Ma, Y. Wang, Y. Tian, D. Wu, X. Li, Y. Zhang, C. Shan and X. Fang, *Mater. Horiz.*, 2020, **7**, 530–540.
52 J. Li, T. Inoshita, T. Ying, A. Ooishi, J. Kim and H. Hosono, *Adv. Mater.*, 2020, **32**, 2002945.